Novel N-Black $In_2O_{3-x}/InVO_4$ heterojunction for efficient photocatalytic fixation: Synergistic effect of exposed (321) facet and oxygen vacancy

Jin Ye,[a] Jiating Xu,*[a] Chunsheng Li,[a] Di Tian,[b] Xiaohan Zhao,[c] Qiang Wang,[a] Wubin Lv,[a] Jun Wang,[a] Haijiao Xie,[e] Yudong Li,[d] Zhiguo Liu,[a] and Yujie Fu*[a]

[a] Key Laboratory of Forest Plant Ecology, Ministry of Education, College of Chemistry, Chemical Engineering and Resource Utilization, Northeast Forestry University, Harbin 150040, P. R. China

[b] Key Laboratory of Jiangxi Province for Persistent Pollutants Control and Resources Recycle, Nanchang Hangkong University, Nanchang 330063, P. R. China

[c] Jiangsu Key Laboratory of Advanced Catalytic Materials and Technology, School of Petrochemical Engineering, Changzhou University, Changzhou 213164, PR China

[d] Key Laboratory of Bio-Based Material Science and Technology of Ministry of Education, Northeast Forestry University, Harbin, 150040, P. R. China

[e] Hangzhou Yanqu Information Technology Co. Ltd, Xihu District, Hangzhou 310003, P. R. China

1. Characterization

The structures of the composites were recorded at a scanning rate of 12 º/min using X-ray diffraction (XRD, D8 Focus) with Cu Kα radiation (λ=1.5406 Å). The morphology of the composite was observed by scanning electronic micrograph (SEM, Nova Nano SEM 450) and Transmission electron microscope (TEM, FEI TalosF200x). The optical property of the composite was characterized using UV-visible (UV-vis) diffuse reflectance spectroscopy (Varian Cary300). Photoluminescence (PL) spectroscopy was recorded *via* an Agilent Cary Eclipse (F-7000) at room temperature. Time-resolved photoluminescence (TRPL) spectra for samples were conducted from 350 to 600 nm with a photoluminescence spectrometer (QM8000) at an excitation 325 nm. $BaSO_4$ was used as a reflectance standard in the UV-vis diffuse reflectance experiment. The chemical composition and element valence were analyzed using X-ray photoelectron spectroscopy (XPS, Kratos Axis Ultra) with a monochromated Al Kα X-ray source (hν=1486.6 eV). Raman spectroscopy was carried out by Confocal Laser Raman Spectrometer (DXR Raman) at an excitation 532 nm. N_2 adsorption-desorption isotherm measurements were investigated to study the Brunauer-Emmett-Teller (BET) specific surface areas of the samples. All electrochemical and photoelectrochemical characterizations were performed on an electrochemical workstation (CHI760E) using a three-electrode system (pH 7.0) with Pt as the counter electrode, Ag/AgCl as the reference electrode, and ITO as the working electrode under visible light. In Mott-Schottky plots, the test frequency is 500, 1000 and 1500 Hz and the potential range is -1 to 0.8 V. The

electron spin resonance (ESR) spectra were performed on a Bruker A300 spectrometer at room temperature. Transient photocurrent response measurements were tested on an electrochemical workstation in the saturated solution of Na_2SO_4 (0.5 M) with 20 s interval under visible light by controlling the light on and off. The in situ diffuse reflectance flourier transform infrared spectroscopy (In-situ DRFTIRS) spectra were investigated by in situ FTIR spectrometer (Thermo iS50FT-IR) with MCT detector and designed reaction cell. Electrochemical impedance spectroscopy (EIS) was carried out in the frequency range of 0.01 to 10^5 Hz by electrochemical workstation with Nafion solution. Nitrogen temperature-programmed desorption (N_2-TPD) was conducted on a Micromeritics AutoChem II 2920 instrument. The concentrations of NH_4^+, NO_3^- and NO_2^- was quantified by ion chromatography (930 compact IC Flex, Metrohm). UV-vis absorption spectra of the samples were recorded on a Shimadzu UV-2550 UV-vis spectrometer. The 300W Xenon lamp (PLS-SXE 300, Beijing Perfect Light Co., Ltd.) was used as the light source. The products from isotopic labeling experiments were analyzed by high-resolution mass spectrometry (Bruker Apex IV Fourier Transform Mass Spectrometer). And Ultraviolet photoemission spectroscopy (UPS) measurements were performed on a Thermo Fisher ESCALAB 250Xi instrument with a He radiation source ($h\nu$ = 21.2 eV). From UPS spectra, the work function Φ of sample was calculated according to the equation $\Phi = h\nu - (E_{Fermi} - E_{cutoff})$, in which $h\nu$ is the He I energy (21.2 eV).[1]

2. Photocatalytic N_2 fixation performance test

Photocatalytic N_2 fixation performance for all sample were investigated by all glass

automatic on-line trace gas analysis system (Labsolar 6A, Beijing Perfectlight Technology Co., Ltd.) with ambient conditions under visible light using 300 W Xenon lamp as light source. In a simple experiment, 50 mg photocatalyst and 100 mL deionized water were added into the reactor to form a uniform suspension *via* sonication. After that, a circulating water system was carried out to maintain room temperature. Subsequently, high-purity nitrogen was bubbled into the above solution in darkness for 30 min with continuously stirring and then reacted under light irradiation with 300 W Xe lamp. Finally, 5 mL of the suspension was withdrawn per 30 min and the liquid sample was filtered through 0.22 μm filter to remove the photocatalyst. Nessler's reagent was used as chromogenic agent, and the concentration of NH^{4+} was tested at 420 nm in the spectrophotometer.

3. Isotopic labeling experiments

Isotopic labeling experiments were performed to further verify the nitrogen source of NH^{4+} originated from dissolved N_2 using $^{15}N_2$ by the indophenol blue method. Isotopic labeling experiments were similar to above photocatalytic N_2 fixation performance test. The catalyst suspension including 50 mg photocatalyst and 100 mL deionized water) was continuously stirred in the dark. Then, high-purity Ar was bubbled through the suspension for 30 min to remove dissolved N_2 in the aqueous suspension. Furthermore, $^{15}N_2$ was continuous bubbled in reaction solutions. The reaction solutions were analyzed through the Nessler's reagent. The products were analyzed by high-resolution mass spectrometry (Bruker Apex IV Fourier Transform Mass Spectrometer) and 1H nuclear magnetic resonance (^{1}HNMR, JEOL JNM-

ECZ400S).

4. Free radical capture experiment

Free radical capture experiments were employed to verify the roles of different reactive oxygen species. In a typical method, 10 mg of photocatalyst was suspended in 100 mL aqueous solution of MB (10 mg/L). After 30 min of adsorption/desorption equilibrium, the photocatalytic degradation of MB was initiated by irradiating the reaction mixture with different scavengers such as tert-butanol (t-BuOH), benzoquinone (BQ), and disodium ethylenediaminetetraacetate (EDTA) as scavengers for $\cdot OH$, $\cdot O_2^-$ and h^+ were added into the photocatalytic reaction process, respectively. Photodegradation was monitored by measuring the absorbance of the solution at 664 nm.

5. ESR spin-trapping experiments

In a typical experiment, 20 mg of photocatalyst was dispersed in 5 mL of ultrapure water/methyl alcohol under ultrasonic for 30 min. Then, 10 μL of 5,5-dimethyl-1-pyrroline-N-oxide (DMPO) and 2,2,6,6-Tetramethylpiperidine (TEMP) were added into above solution for $\cdot OH$ and $\cdot O_2$ with ultrasonic dispersion, respectively. The sample was loaded in a capillary tube and further placed into a quartz nuclear magnetic tube before subjecting to ESR test.

6. Computational methods

We have employed the Vienna Ab initio Simulation Package (VASP) to perform all density functional theory (DFT) calculations within the generalized gradient approximation (GGA) using the Perdew-Burke-Ernzerhof (PBE) functional. We have

chosen the projected augmented wave (PAW) potentials to describe the ionic cores and take valence electrons into account using a plane wave basis set with a kinetic energy cutoff of 400 eV. Geometry optimizations were performed with the force convergency smaller than 0.03 eV/Å. The original bulk structures In_2O_3 has been optimized before the construction of surfaces with the Monkhorst-Pack k-point of 2×2×2. The In_2O_3 (321) surfaces with 48 In and 72 O atoms and In_2O_3 (222) surfaces with 48 In and 72 O atoms were applied with half of the surface at the bottom fixed in all the calculations. The oxygen vacancy on the In_2O_3 (321) and In_2O_3 (222) surface was created by removing two surface O atom from the perfect surface. Monkhorst-Pack k-points of 2×2×1 and 1×2×1 were applied for all the surface calculations for and In_2O_3 (222) and In_2O_3 (321), respectively. The surface energy of (222) and (321) planes for In_2O_3 were determined as follows:

$$E(total) = E(perfect) - E(O_2)-2\times E(bulk)/3 \quad (1)$$

$$E(surface\ energy) = E(total)/(surface\ area\times 2) \quad (2)$$

(Where E(total), E(perfect), $E(O_2)$ and E(bulk) are total energy, energy of perfect surface, energy of O_2 and bulk energy of In_2O_3, respectively.)

Of course, calculation of adsorption energy for NH_3 of different crystal planes for In_2O_3 were determined as follows:

$$E(adsorption\ energy) = E(absorb+slab) - E(slab) - E(N_2/NH_3) \quad (3)$$

(Where E(absorb+slab), E(slab) and $E(N_2/NH_3)$ are the energy of adsorbed system, the energy of the clean substrate surface and the energy of the adsorbates, respectively.)

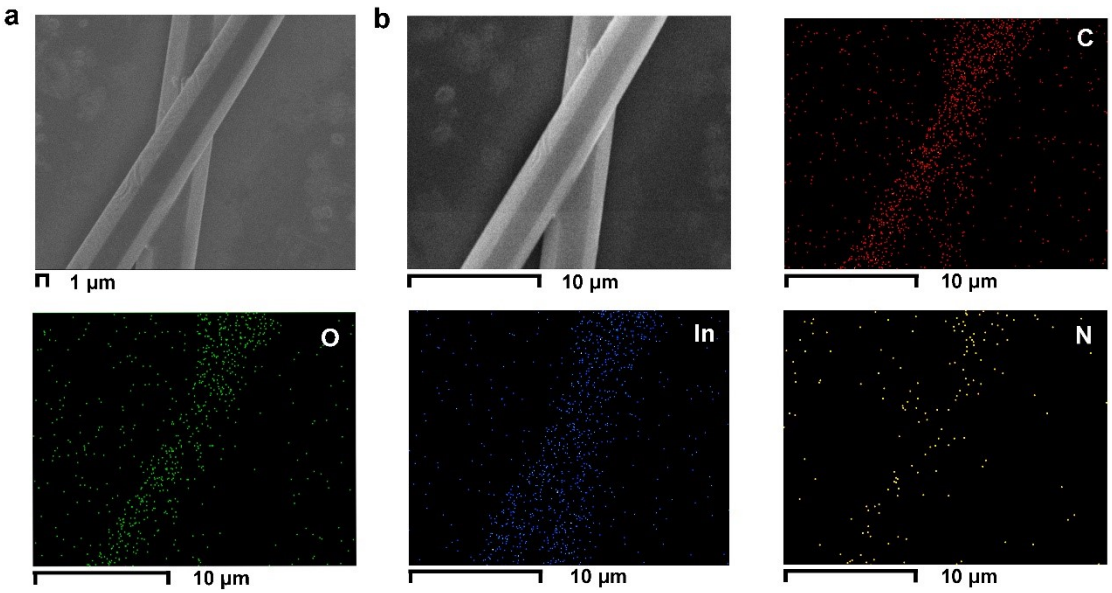

Fig. S1 SEM images of the NH_2-MIL-68 (a, b) and corresponding EDS mapping.

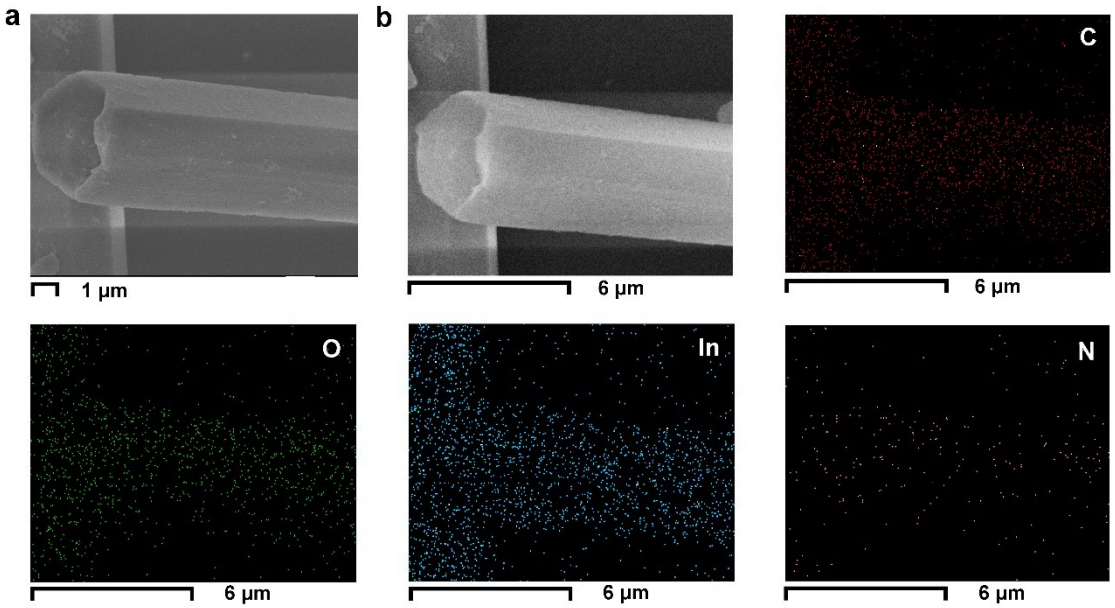

Fig. S2 SEM images of the N-In_2O_3 (a, b) and corresponding EDS mapping.

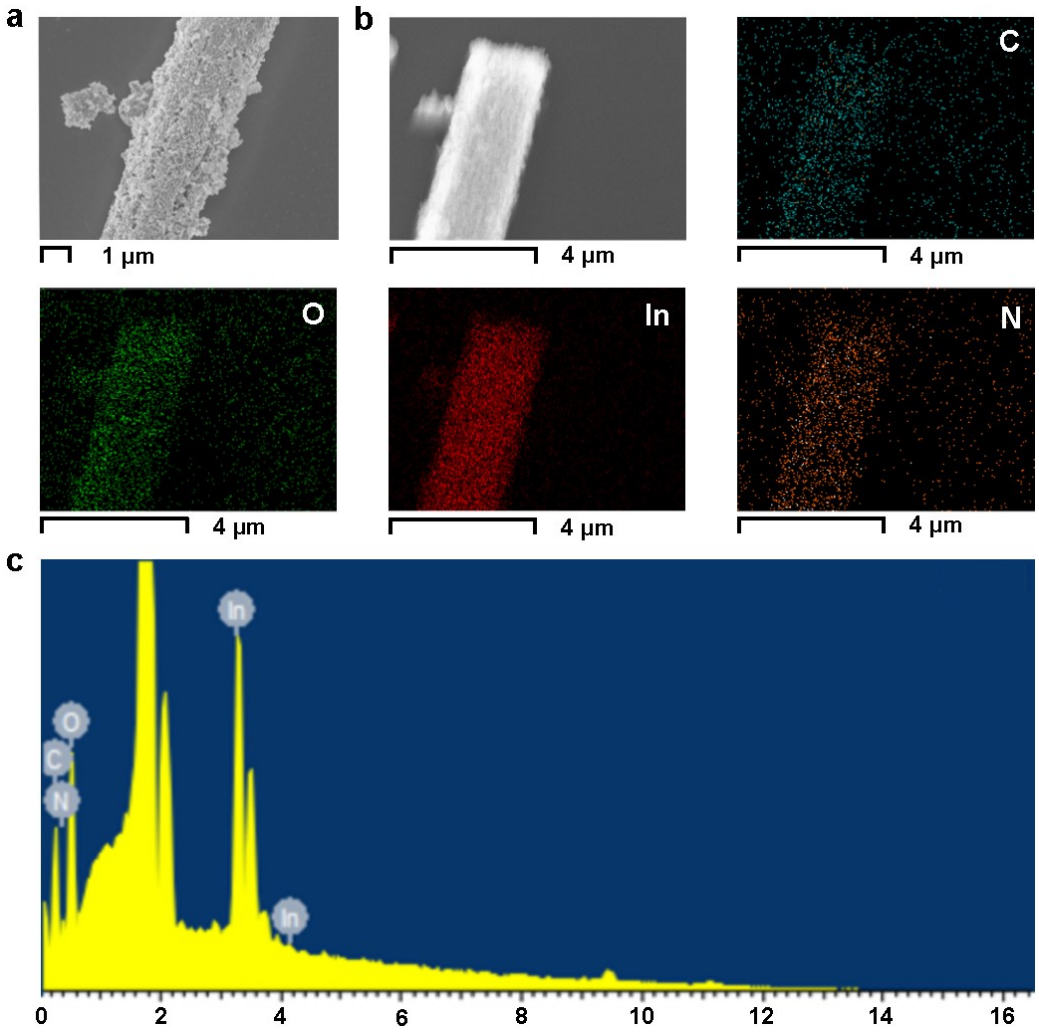

Fig. S3 SEM images of the N-Black-In_2O_3 (a, b) and corresponding EDS mapping, EDS of the N-Black-In_2O_{3-x} (c).

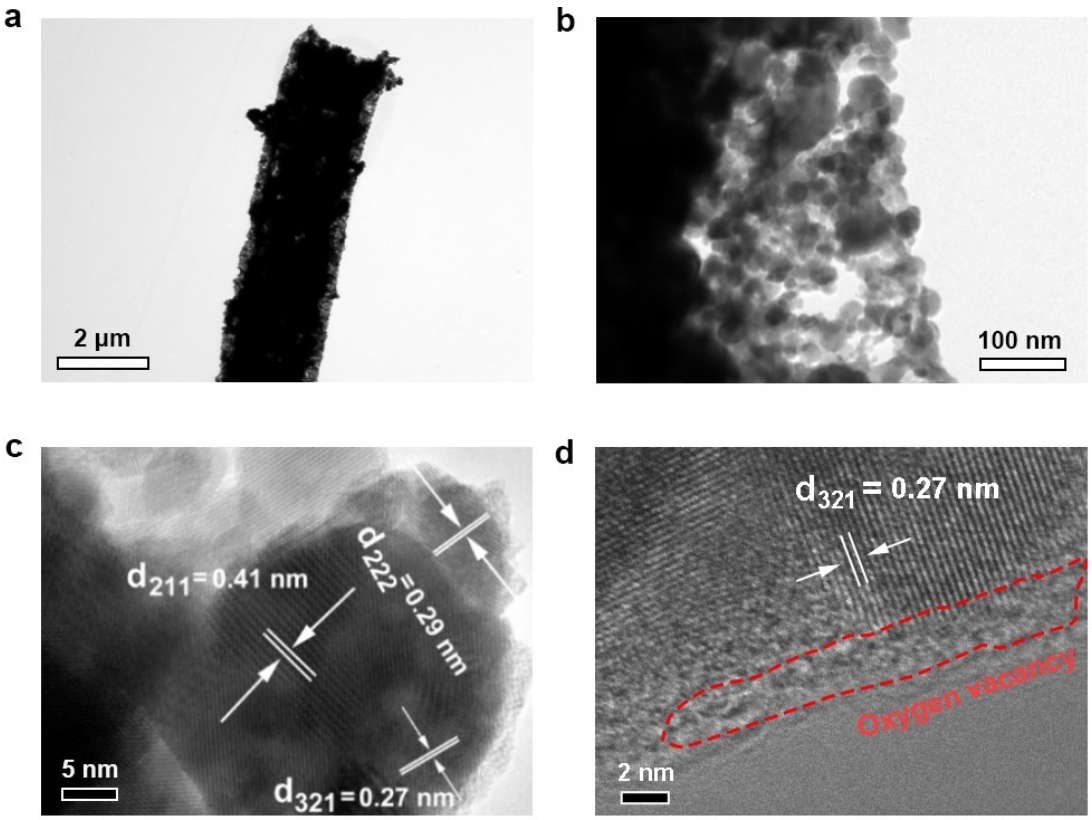

Fig. S4 TEM (a-b) and HRTEM (c-d) images of the N-Black-In_2O_{3-x}.

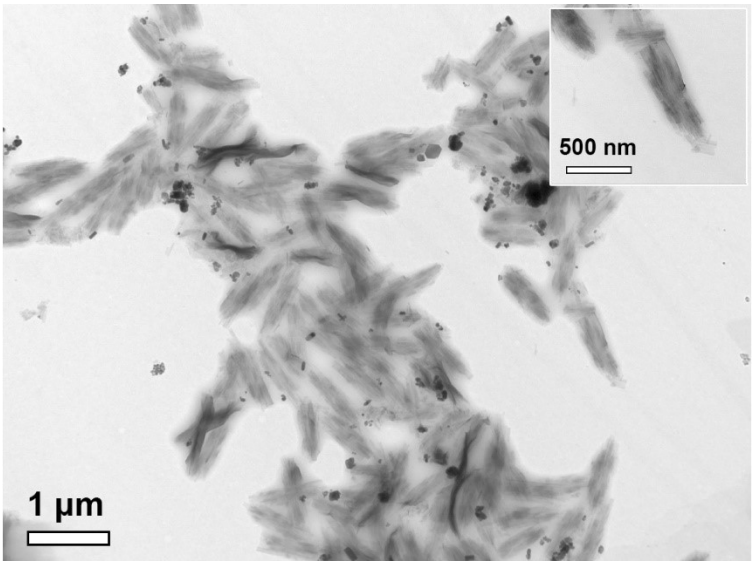

Fig. S5 TEM images of the $InVO_4$ nanosheets and enlarge image (inset).

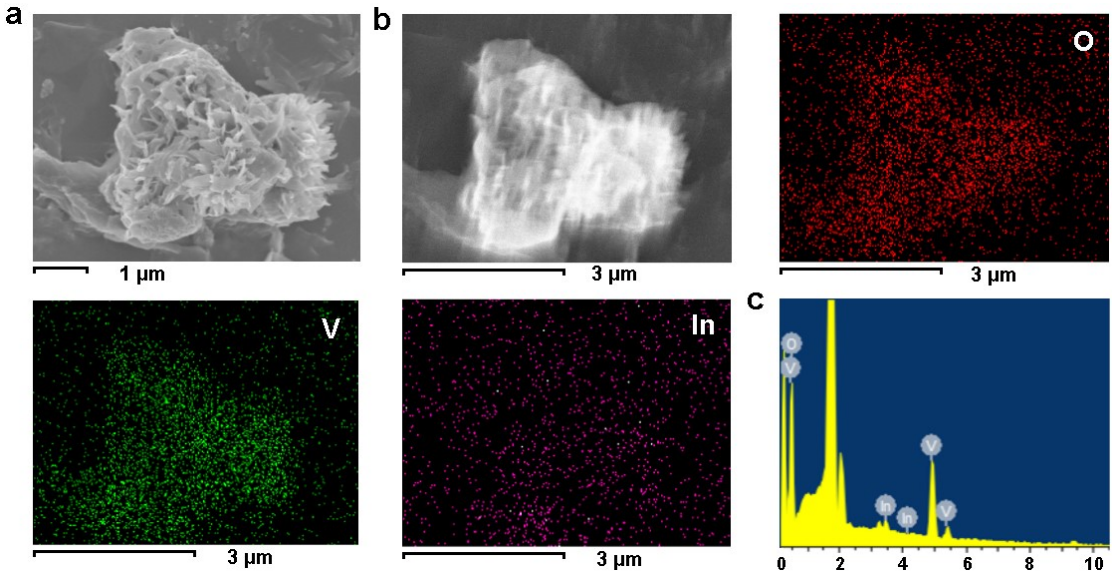

Fig. S6 SEM images of the $InVO_4$ nanosheets (a, b) and corresponding EDS mapping, EDS of the $InVO_4$ (c).

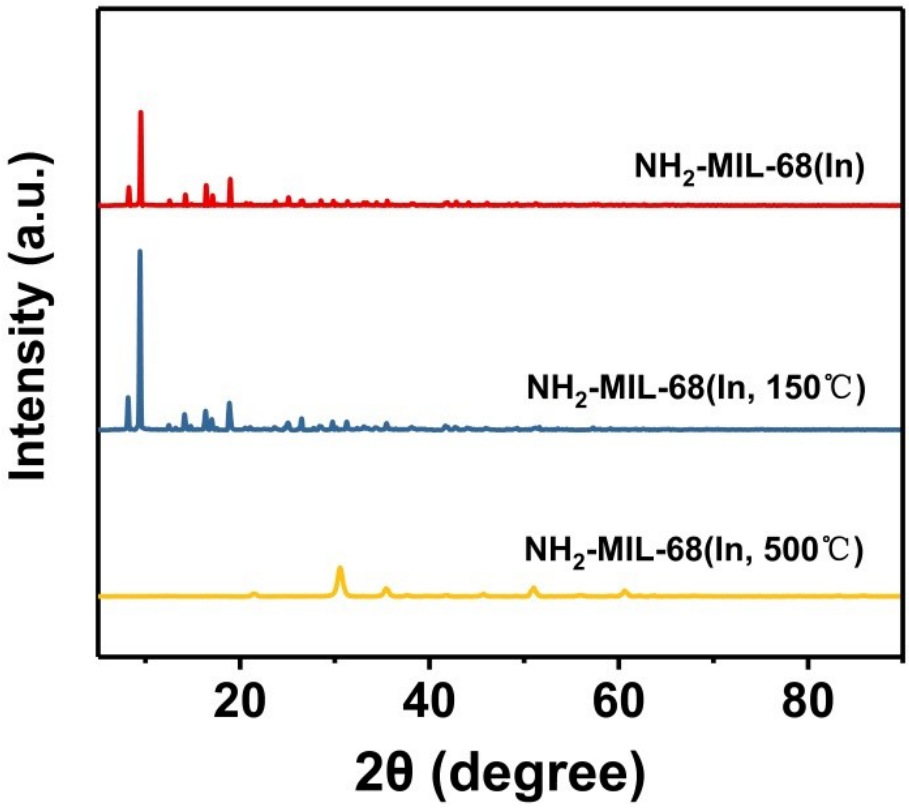

Fig. S7 XRD patterns of NH_2-MIL-68 at different calcination temperatures.

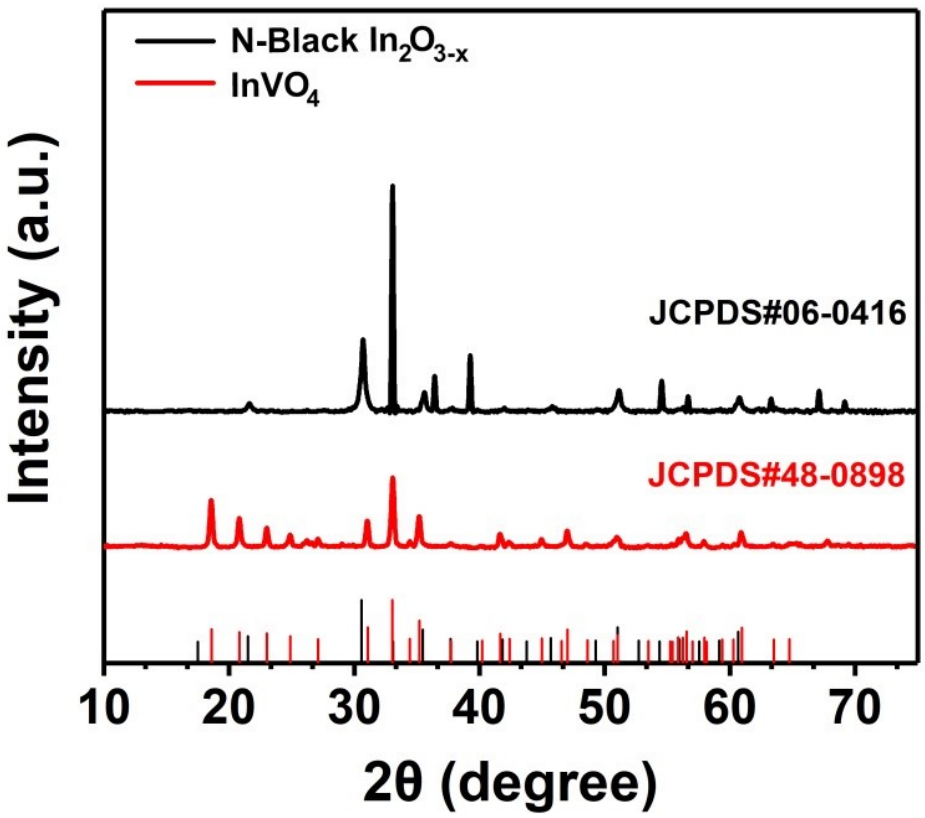

Fig. S8 XRD patterns of N-Black In_2O_{3-x} and $InVO_4$.

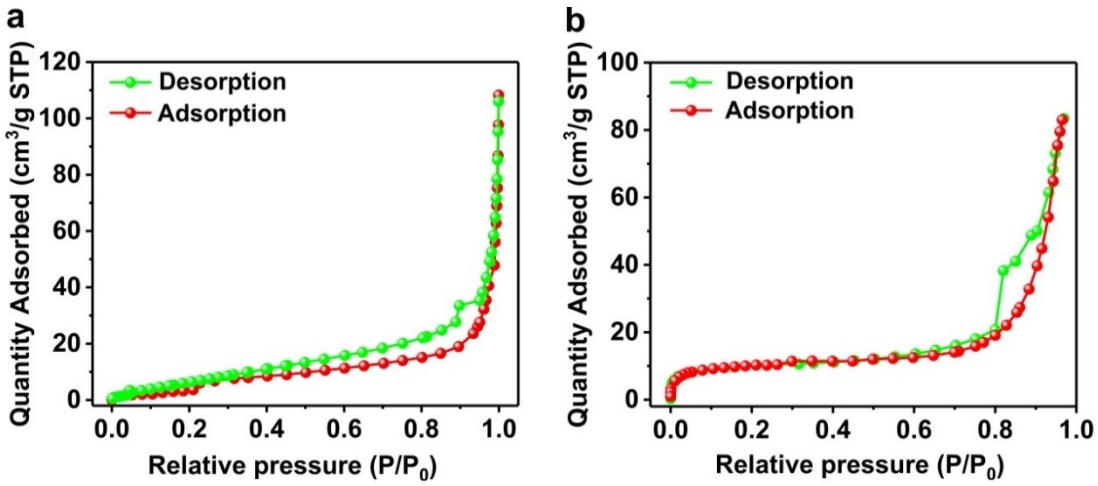

Fig. S9 N_2 adsorption-desorption isotherms of N-Black In_2O_{3-x} (a), N-Black $In_2O_{3-x}/InVO_4$ (b).

Table S1. The specific surface area and average pore diameter for N-Black In_2O_{3-x} and N-Black $In_2O_{3-x}/InVO_4$.

Sample	**BET surface area (m^2/g)**	**Average pore diameter (nm)**
N-Black In_2O_{3-x}	37.6	13.7
N-Black $In_2O_{3-x}/InVO_4$	10.5	32.3

Fig. S10 The picture of the prepared NH_2-MIL-68 (a), N-In_2O_3 (b), N-Black In_2O_{3-x} (c) and $InVO_4$ (d) samples.

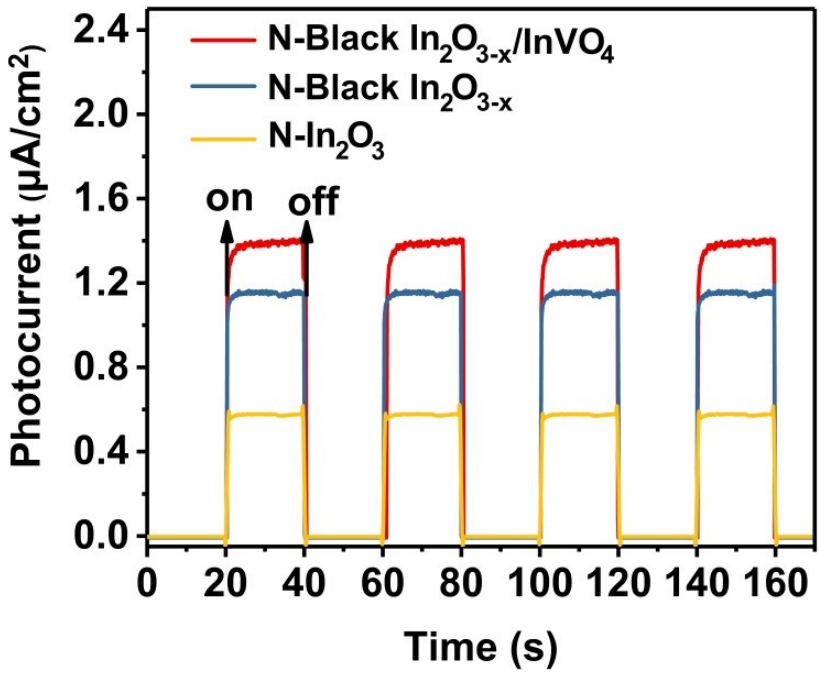

Fig. S11 Photocurrent transient responses of N-In_2O_3, N-Black In_2O_{3-x} and N-Black $In_2O_{3-x}/InVO_4$.

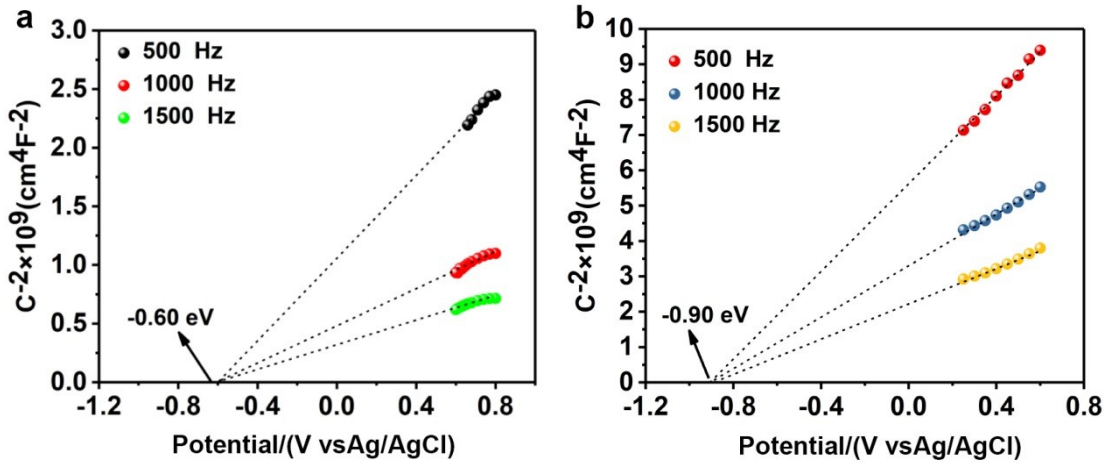

Fig. S12 Mott-Schottky plots of N-Black In_2O_{3-x} (a) and $InVO_4$ (b).

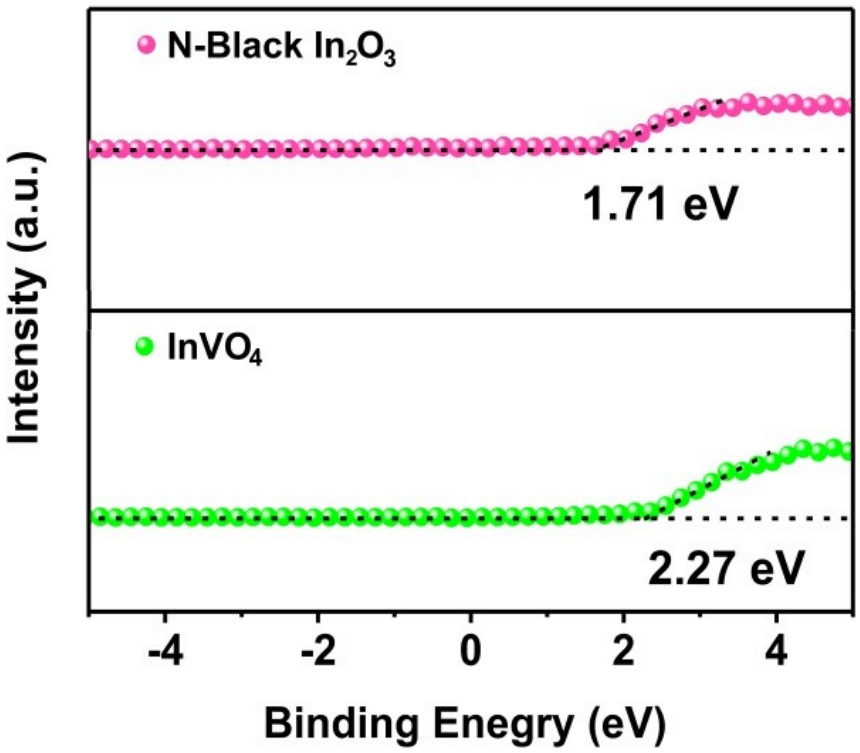

Fig. S13 XPS valence band spectra of N-Black In_2O_{3-x} and $InVO_4$.

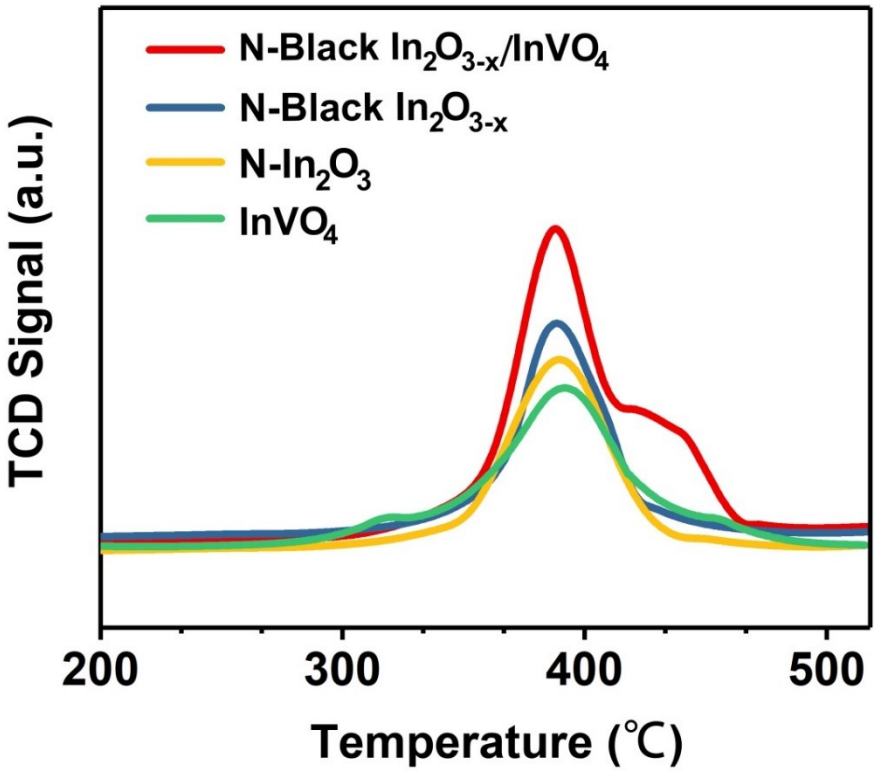

Fig. S14 N_2-TPD profiles of the as-prepared samples

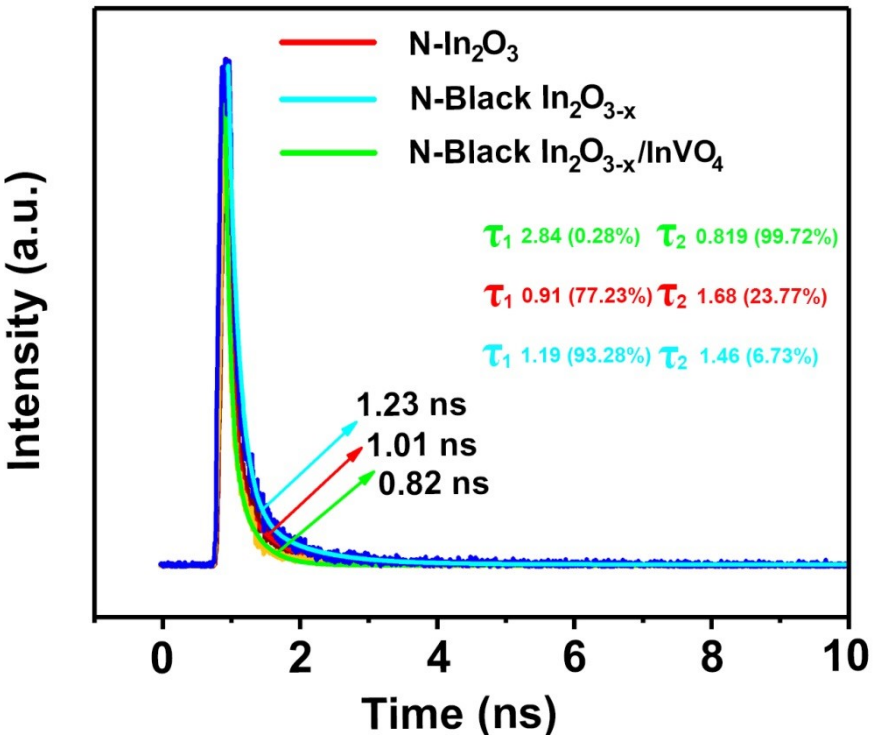

Fig. S15 Time-resolved transient PL decay for N-In_2O_3, N-Black In_2O_{3-x} and N-Black $In_2O_{3-x}/InVO_4$. Fitting parameters and results refer to the following formula：

$$\tau = \frac{A_1\tau_1^2 + A_2\tau_2^2}{A_1\tau_1 + A_2\tau_2}$$

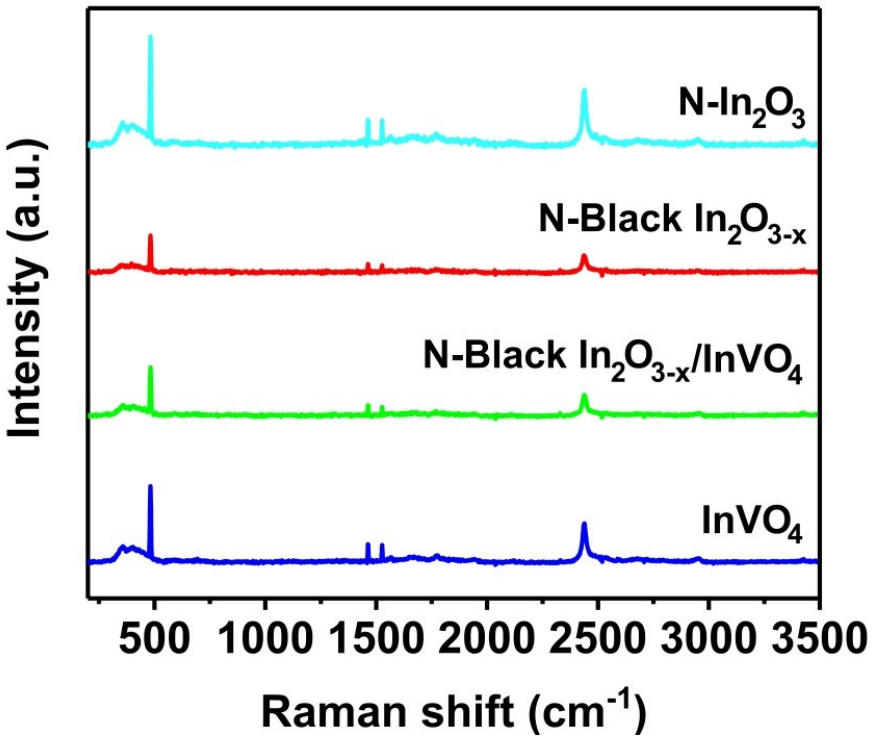

Fig. S16 Raman spectroscopy for N-In_2O_3, N-Black In_2O_{3-x} and N-Black $In_2O_{3-x}/InVO_4$.

Fig. S17 Evaluation of photocatalytic nitrogen fixation tests by Labsolar 6A.

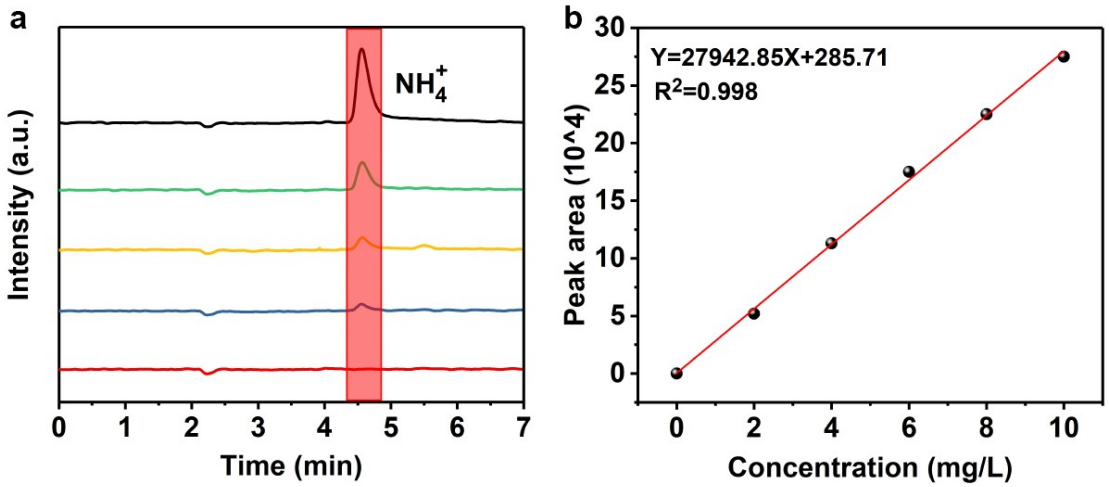

Fig. S18 Spectra of ion chromatography for ammonia solution with different concentrations (a), the standard curve for NH_4^+ detection via ion chromatography method (b).

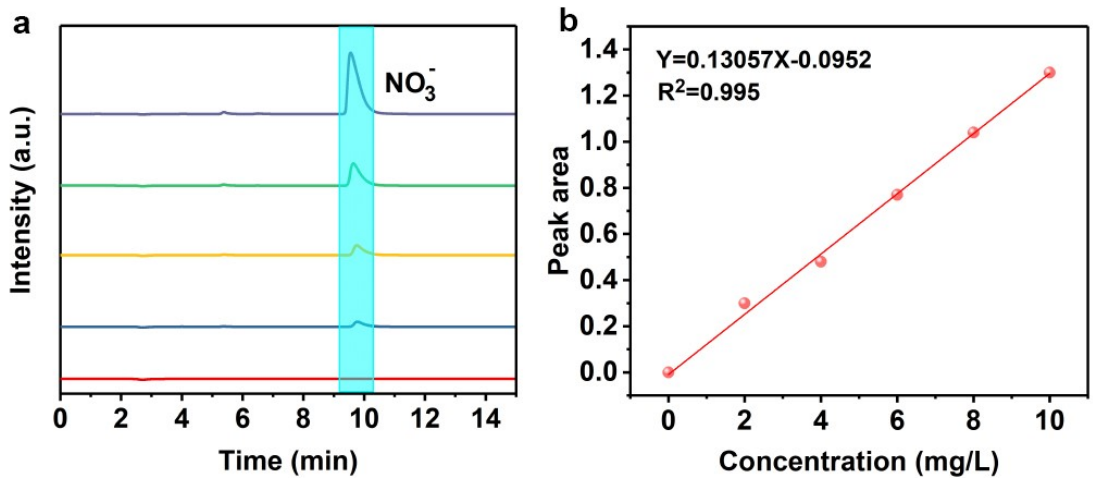

Fig. S19 Spectra of ion chromatography for ammonia solution with different concentrations (a), the standard curve for NO_3^- detection via ion chromatography method (b).

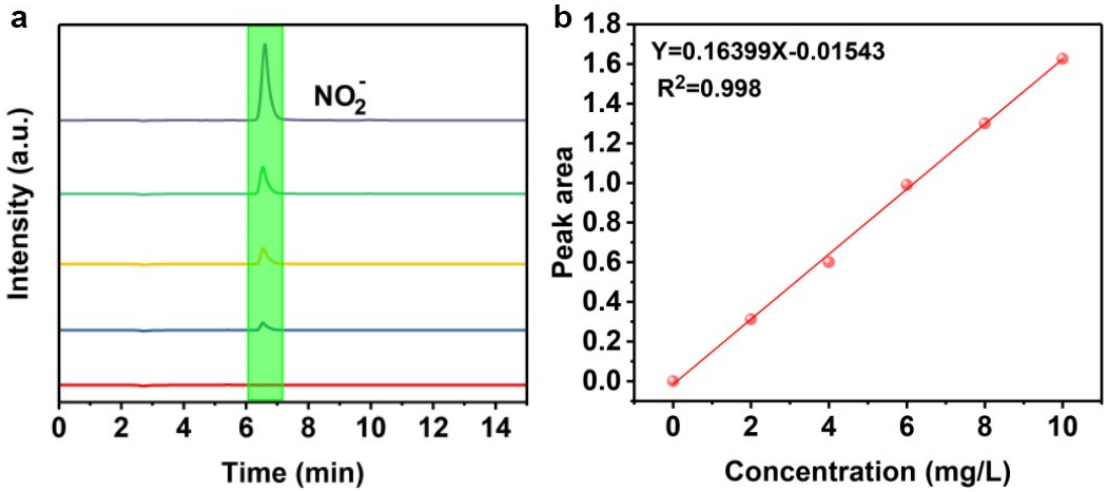

Fig. S20 Spectra of ion chromatography for ammonia solution with different concentrations (a), the standard curve for NO_2^- detection *via* ion chromatography method (b).

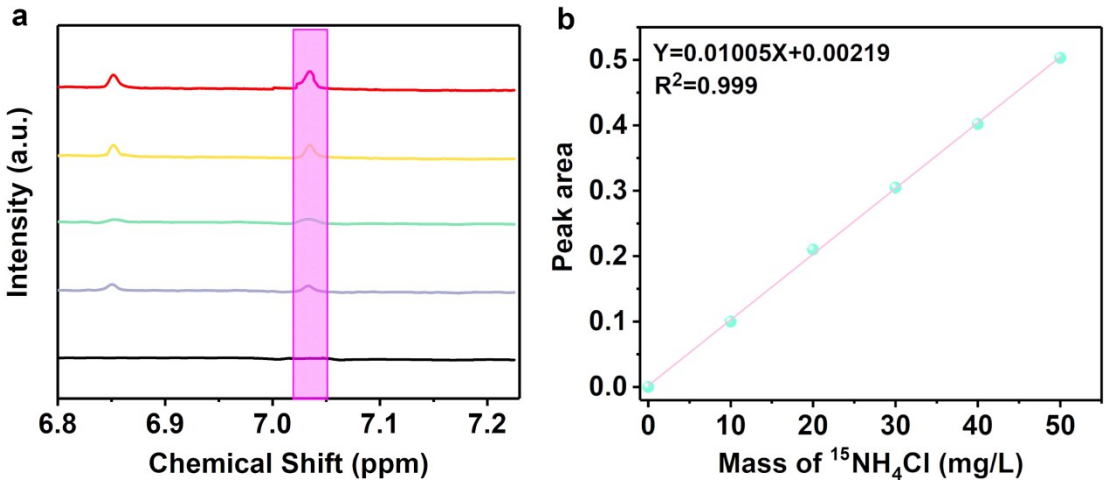

Fig. S21 ^{1}H-NMR spectra of different amount of $^{15}NH_4Cl$ (a), the standard curve of the mass of $^{15}NH_4Cl$ vs. area of peak in ^{1}HNMR spectra (b).

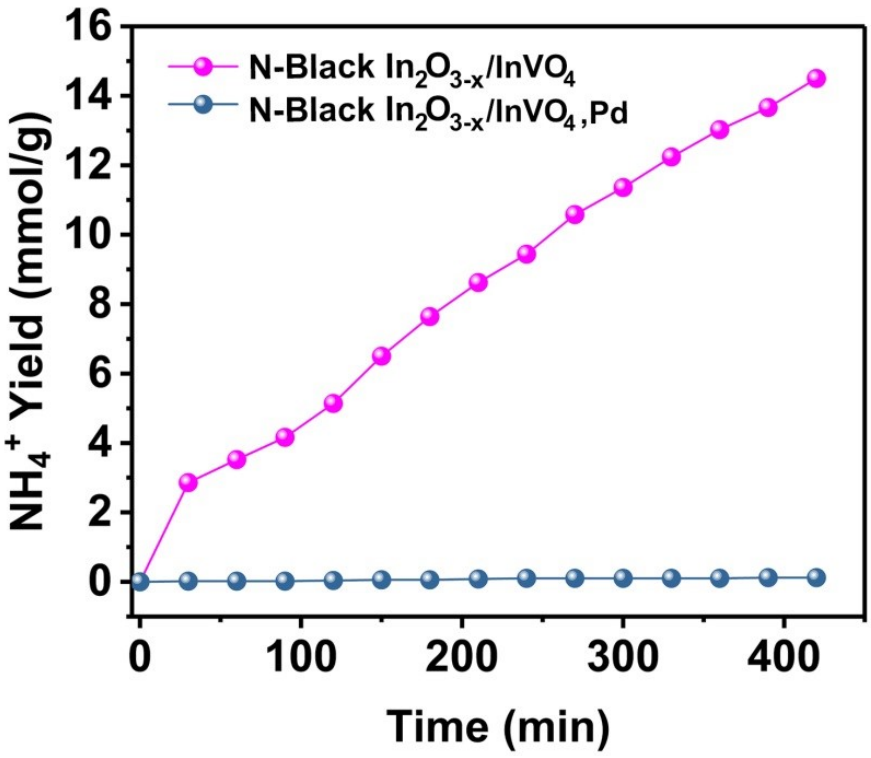

Fig. S22 Photocatalytic nitrogen fixation tests for N-Black $In_2O_{3-x}/InVO_4$ heterostructure with or without Pd.

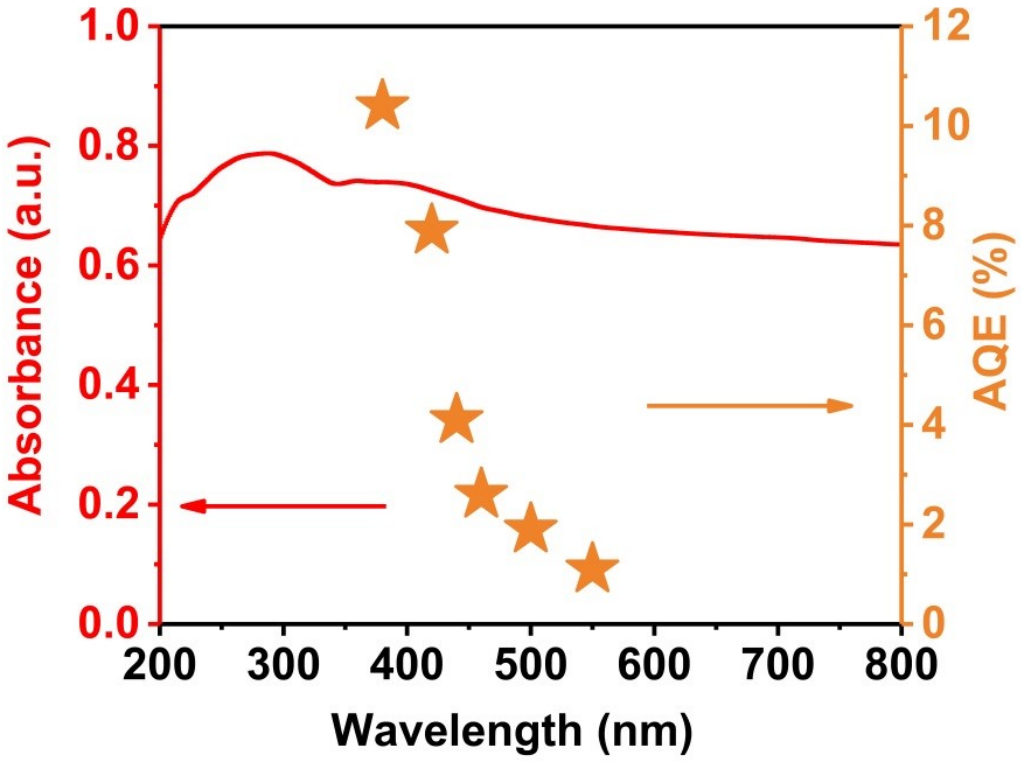

Fig. S23 The AQE of H_2 evolution for N-Black $In_2O_{3-x}/InVO_4$ under monochromatic lamp irradiation at different wavelengths.

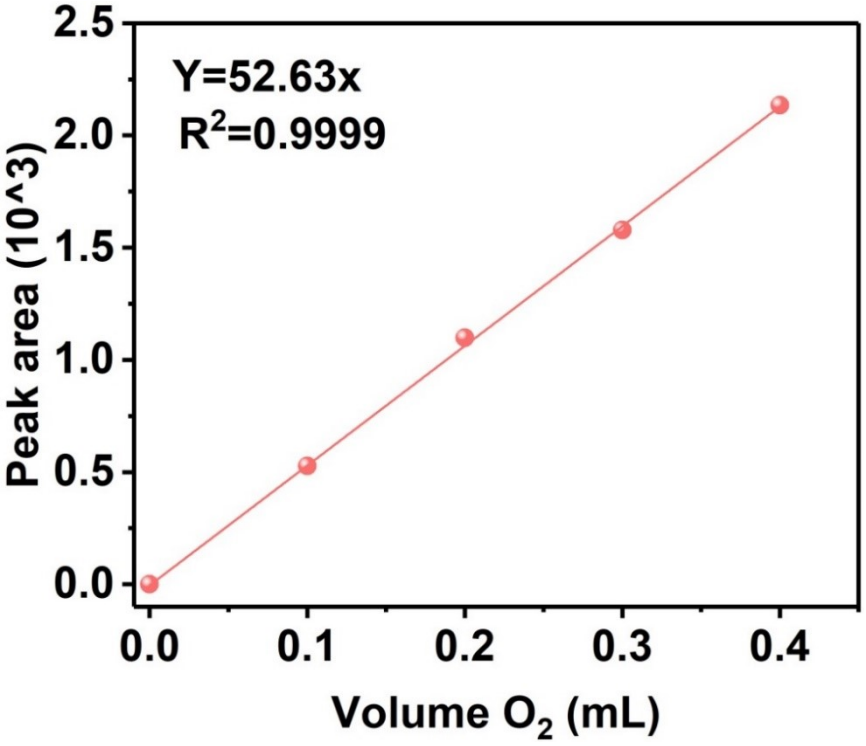

Fig. S24 The plot of volume of O_2 gas vs. the corresponding chromatographic peak area.

Table S2. The calculated ammonia production rates based on different detection methods.

Catalysts	**Light source**	**NH_3 yield (mmol g^{-1} h^{-1})**		
N-Black $In_2O_{3-x}/InVO_4$	> 400 nm (300 W)	Nessler's reagent	Ion chromatograph	^{1}HNMR
		2.07	1.96	1.92

The NH_4^+ yields are calculated about 2.07 mmol g^{-1} h^{-1} under visible light by Nessler's reagent method. And the NH_4^+ yields are computed for 1.96 mmol g^{-1} h^{-1} under visible light by the ion chromatographic data (**Fig. S18**). Furthermore, NH_4^+ yields are calculated about 1.92 mmol g^{-1} h^{-1} by ^{1}HNMR method. As a result, the ion chromatography data are in accordance with the results obtained by the Nessler's reagent method. Meanwhile, in the isotope experiment, pure $^{15}N_2$ was employed as a nitrogen source in photocatalytic N_2 fixation process with N-Black $In_2O_{3-x}/InVO_4$ as catalyst under visible light (**Fig. S30**). A chemical shift of 7.06 ppm, double peaks with a coupling constant of 73.1 Hz was observed, owing to the spin quantum number I = 2 for $^{15}N_2$.[2] On the contrary, $^{14}N_2$ was also employed as well, a strong triplet signal with a coupling constant of 51.8 Hz was obtained, which strongly confirm that the ammonia in the product comes from the reduction of nitrogen. This result can strongly confirm that the NH_4^+ in the product comes from the reduction of nitrogen.

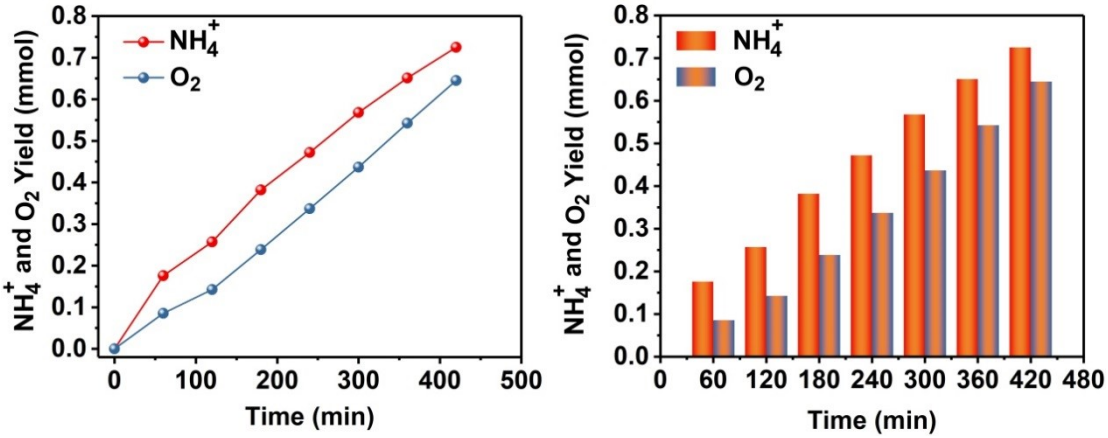

Fig. S25 Photocatalytic production of NH_3 and O_2 during the N_2 fixation over N-Black $In_2O_{3-x}/InVO_4$ as the catalyst in pure water without any sacrificial agents.

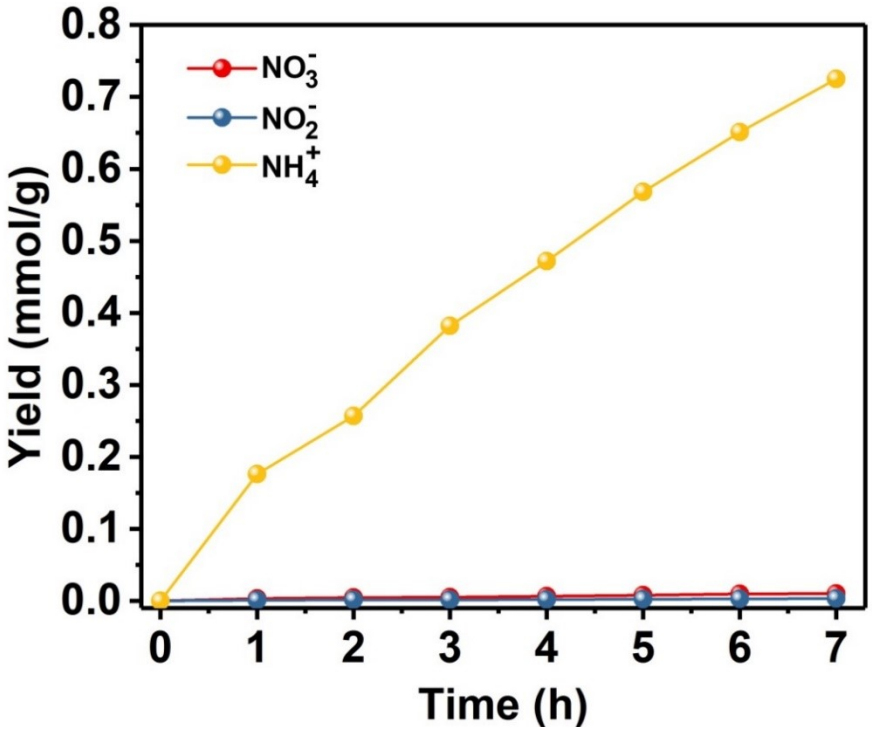

Fig. S26 Photocatalytic nitrogen fixation to NH_4^+, NO_3^- and NO_2^- over N-Black $In_2O_{3-x}/InVO_4$ as detected using ion chromatography.

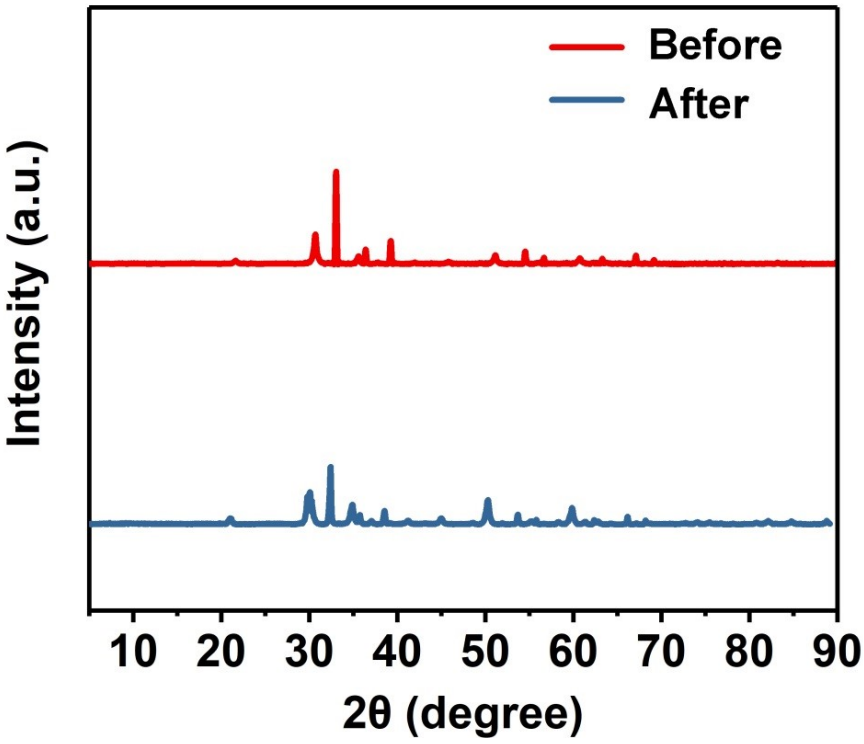

Fig. S27 XRD patterns of the N-Black $In_2O_{3-x}/InVO_4$ sample before and after recycling.

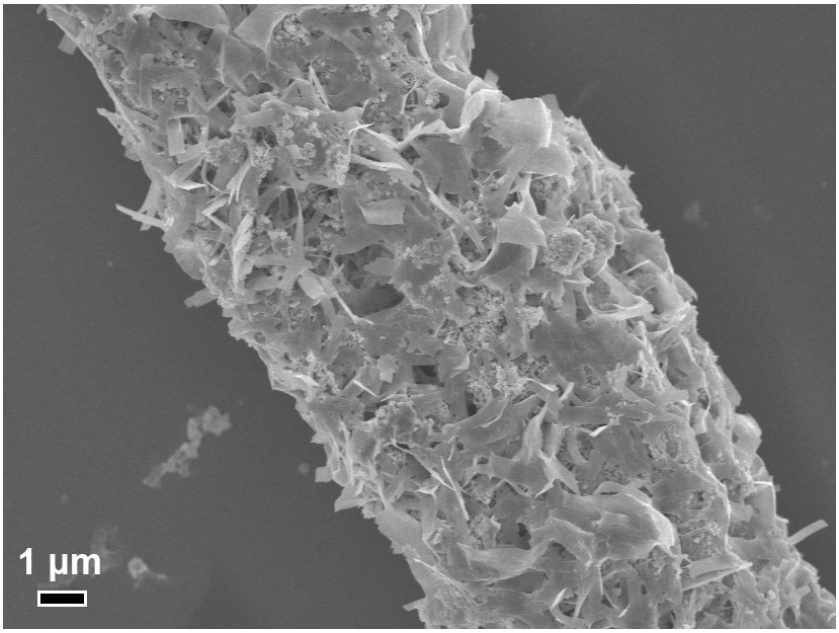

Fig. S28 The SEM image of the N-Black $In_2O_{3-x}/InVO_4$ sample after recycling.

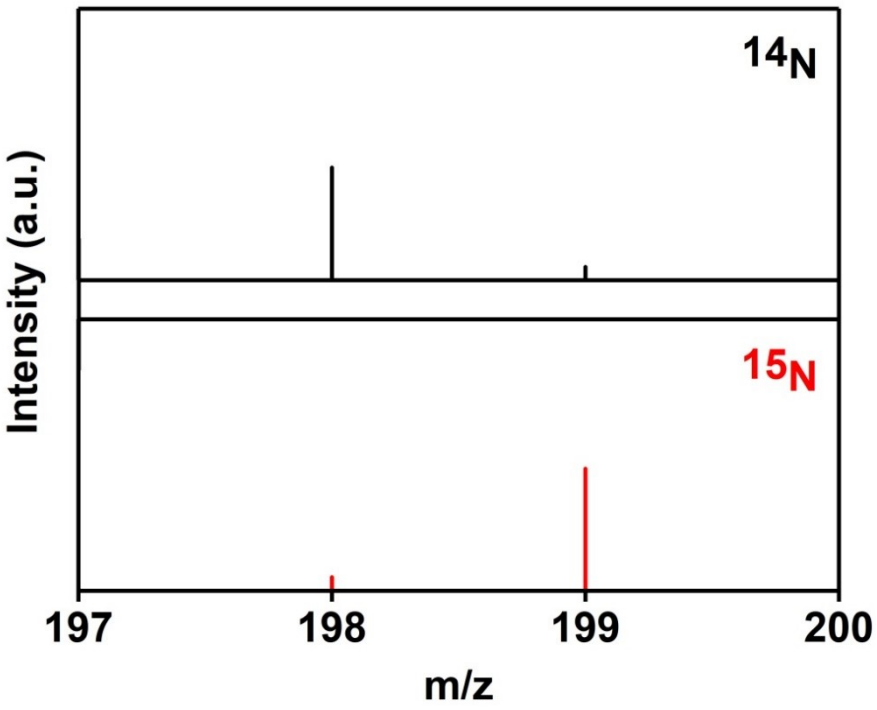

Fig. S29 Mass spectra of the products formed via reaction with indophenol in different reaction atmospheres over N-Black $In_2O_{3-x}/InVO_4$.

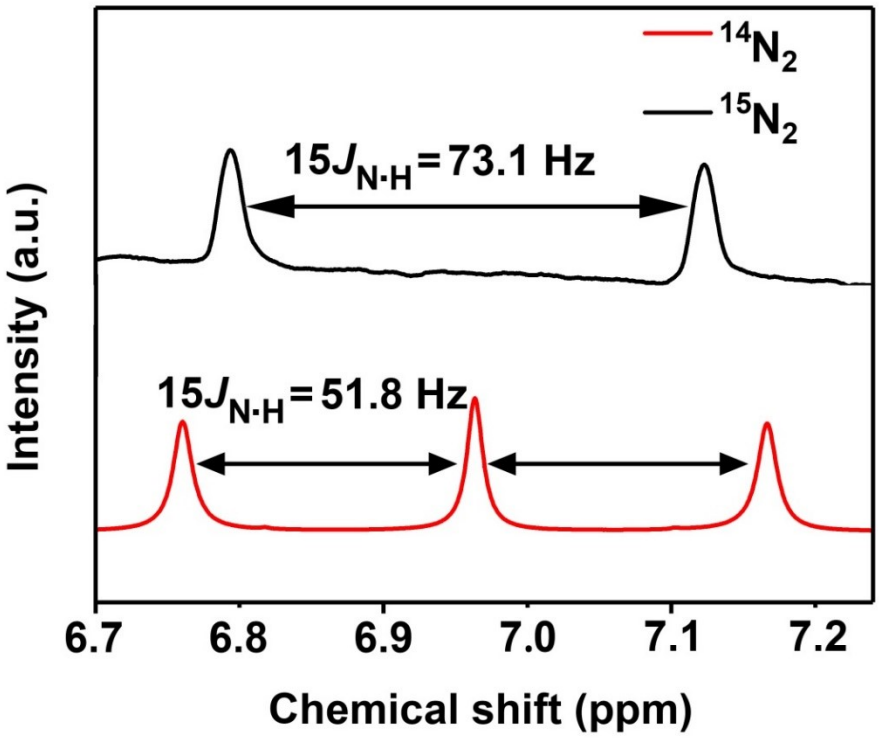

Fig. S30 ^{1}HNMR spectra for produced NH_4^+ over N-Black $In_2O_{3-x}/InVO_4$ using $^{15}N_2$ and $^{14}N_2$ as feeding gas.

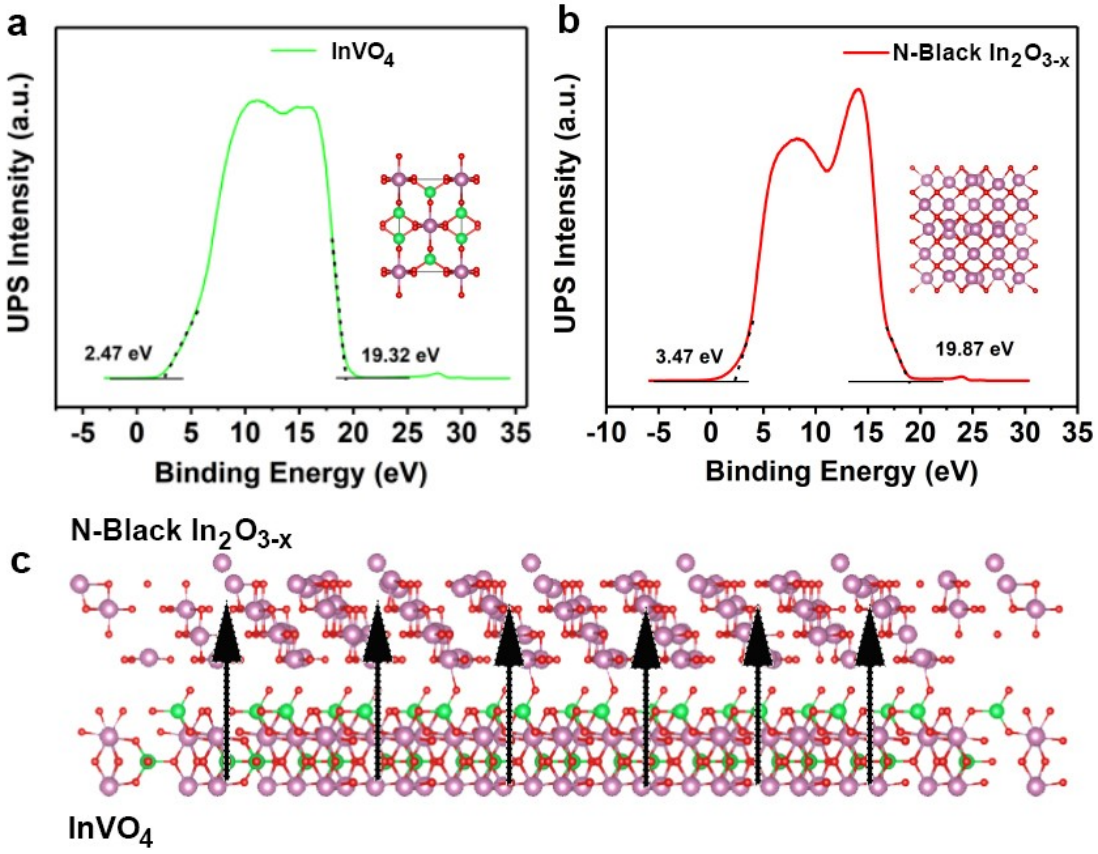

Fig. S31 UPS spectra of $InVO_4$ (a), N-Black In_2O_{3-x} (b) and heterojunction model of N-Black In_2O_{3-x}/$InVO_4$ (c).

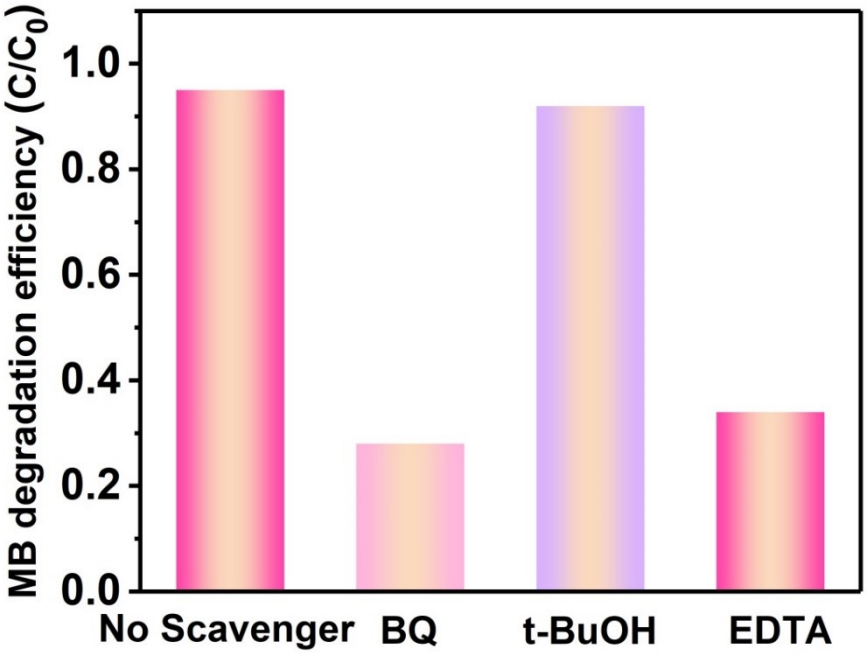

Fig. S32 Photocatalytic activity of N-Black $In_2O_{3-x}/InVO_4$ for the photocatalytic degradation of MB in the presence of different scavengers.

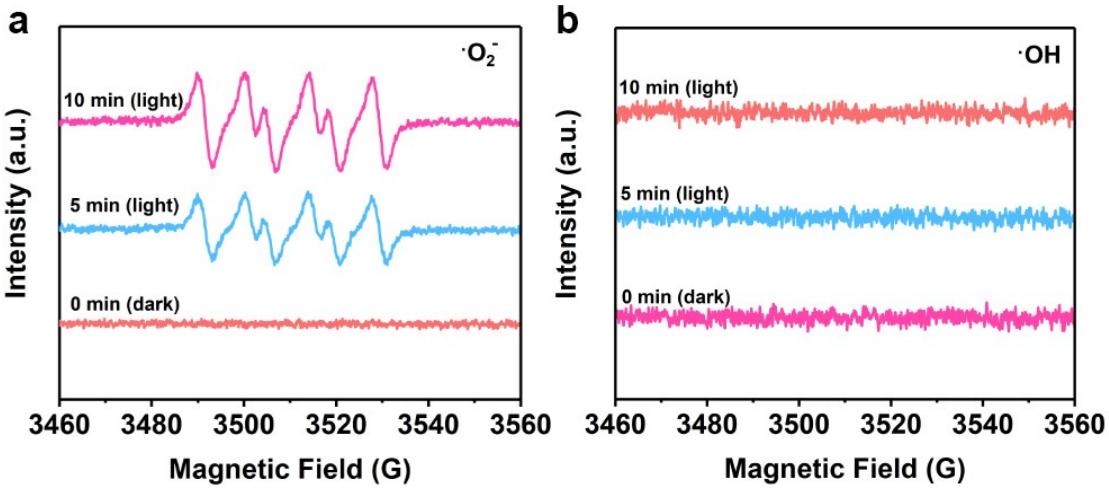

Fig. S33 ESR spectra of N-Black $In_2O_{3-x}/InVO_4$ for $^{\cdot}O_2^-$ (a) and ·OH (b) detection.

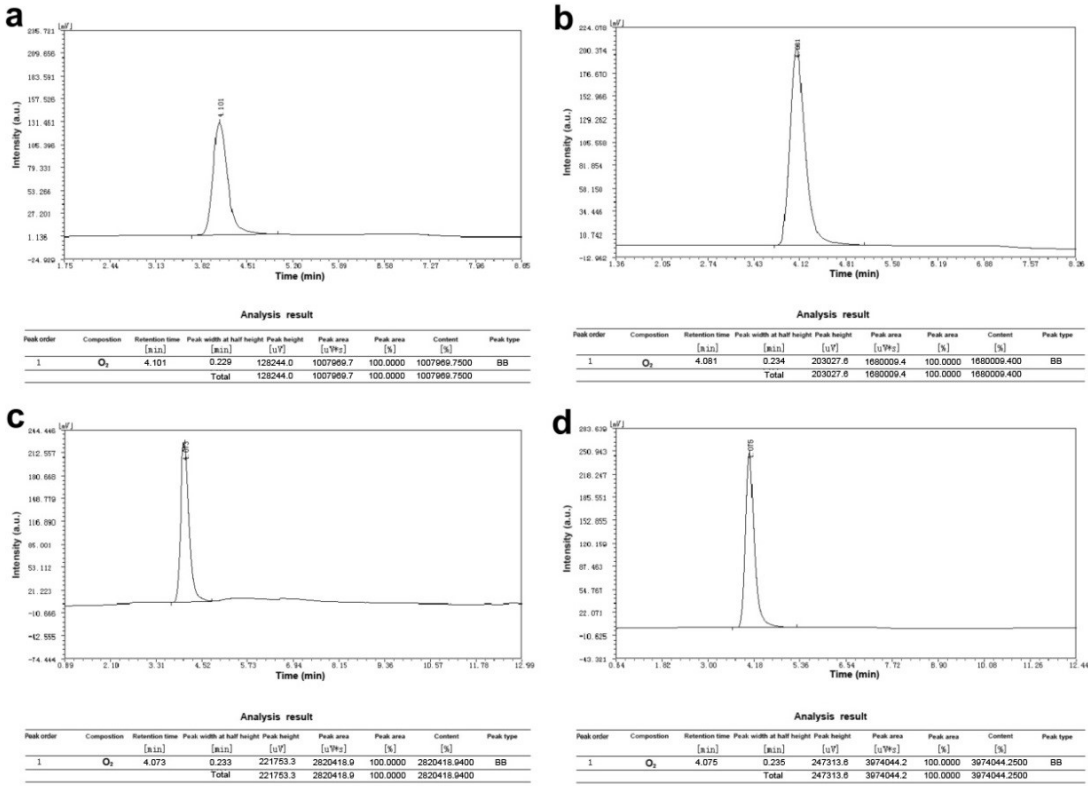

Fig. S34 Evolutions of O_2 production of N-Black $In_2O_{3-x}/InVO_4$ sample for 1 h (a), 2 h (b), 3 h (c), and 4 h (d) under visible-light irradiation.

References

1 J. Liu, J. Zhang, D. Wang, D. Li, J. Ke, S. Wang, S. Liu, H. Xiao and R. Wang, *ACS Sustainable Chem. Eng.*, 2019, **7**, 12428-12438.

2 Y. Liao, J. Qian, G. Xie, Q. Han, W. Dang, Y. Wang, L. Lv, S. Zhao, L. Luo, W. Zhang, H.-Y. Jiang and J. Tang, *Appl. Catal. B* 2020, **273**, 119054.